InTlSb FINAL REPORT

InTlSb for Long-Wavelength Infrared Photodetectors and Arrays

Contract No. N00014-93-1-0409

1997

Manijeh Razeghi
Principal Investigator

Center for Quantum Devices
Dept. of Electrical and Computer Engineering
Northwestern University
Evanston, Illinois 60208

Personnel

Graduate Students:
Y. Choi, J. Kim
Visiting Researchers:
G. Labeyrie
Post-Doctoral Researchers:
E. Kolev, R. Sudharsanan, J. Xu

INTRODUCTION

The objective of this research program is to grow InTlSb alloys for long-wavelength infrared detector applications by low-pressure metalorganic chemical vapor deposition (LP-MOCVD) and to investigate their physical properties. As a first step towards this goal, optimum growth conditions for high quality InSb epitaxial films on InSb, GaAs, and Si substrates have been determined. InSb films grown under these conditions exhibited one of the best structural and electrical properties reported so far[1-3]. For the long-wavelength applications, growth of InAsSb and InTlSb was then carried out using arsine and cyclopentadienylthallium as the source for arsenic and thallium respectively. Growth of InAsSb with appropriate doping resulted in the room temperature operation of InAsSb photodetectors with extended cut-off wavelength[4-6]. Incorporation of thallium into InSb has led to the first successful growth of InTlSb having an extended infrared response[7-10]. By changing the thallium flow, thallium content was varied and the resulting absorption edge varied from 5.5μm to 9.0 μm[11,12]. The photoconductive detectors have been fabricated and measured using Fourier transform infrared (FTIR) spectrometer and blackbody test setup. Using the Hall data, the effective carrier lifetime and detectivity have been calculated for the InTlSb layers. The lifetime value ranged from 10 to 50 ns and detectivity was varied from 2 to 9×10^8cm·Hz$^{1/2}$/W. at 77 K. These results demonstrate InTlSb as feasible material system for long wavelength infrared detection.

Efforts of our research have also been devoted to aspects of materials growth related to photovoltaic detector fabrication. Reproducible epitaxial doping, the foremost requirement to realizing photovoltaic detectors, have been first investigated for InSb. Successful n-and p- type doping were obtained using Sn and Zn as the respective dopants, without any observable degradation. Based on this progress, InSb photovoltaic detectors have been fabricated and measured. As a next step, InAsSb photovoltaic detectors have also been fabricated to investigate the doping and detector performance for the InSb based alloy materials. Device processing technology developed at CQD has been used for the fabrication of InSb and InAsSb photovoltaic detectors and will be applied for the InTlSb detectors later. N- and p-type doping of InTlSb were also achieved to a concentration of 2.5×10^{16}cm^{-3} and 3×10^{18}cm^{-3}, respectively. Because lower doping levels are required for the p-type doping, DEZn replaced DMZn for the Zn source. Lower vapor pressure of DEZn resulted in the lower doping level down to 10^{16}cm^{-3} for InSb and InAsSb resulting in a better doping level control.

MAJOR ACHIEVEMENTS

- Growth of the best (structural and electrical quality) InSb on GaAs substrates. The optimization of the InSb growth condition has been completed.

- Demonstration of the first growth of InTlSb. Evidenced the incorporation of thallium by Auger Electron Spectroscopy. Observed a shift in the absorption edge by infrared transmission and photoresponse.

- Varied thallium content and observed the resulting changes in physical properties.

- Demonstrated InTlSb photoconductor with different Tl compositions. Using the absolute photoresponsivities, effective carrier lifetime and estimated detectivity have been calculated.

- Calibrated the n- and p- type doping level on InSb grown on GaAs using TESn, DMZn and DEZn as dopant sources. Similarity of the doping characteristics for the InAsSb and InTlSb has also been verified.

- Developed device processing technology such as etching, metallization and wire bonding for InSb based materials.

- Demonstrated InSb photovoltaic detectors with different structures (p-i-n and n-i-p). Responsivities have been compared to obtain better structure for the applications.

- Demonstrated p^+-p-n^+ InSb/InAsSb/InSb double heterojunction photodiodes operating at 8-13μm as a step towards the InTlSb photovoltaic detector development.

- Preliminary InTlSb photovoltaic detector has been attempted.

Task 1 Growth of InTlSb

1. Growth of high-quality InSb

Growth

Trimethylindium (TMI) and trimethylantimony (TMSb) were used as precursors. Their respective bubbler temperature were kept at 18 °C and 0 °C. The growths were carried out on InSb, semi-insulating GaAs, and GaAs coated Si substrate. The latter was investigated because of the possibility for future investigation of infrared detection and signal processing circuits on the same substrates. Superclean GaAs and GaAs/Si substrates were directly loaded into the growth chamber without any preparation. During the heating of the substrate, a pregrowth arsine overpressure was maintained in order to prevent any surface degradation. For InSb substrates, the best preparation method was found to be etching in lactic acid : nitric acid (10:1) mixture. However, we observed that this etching reveals line defects on some InSb substrates. The line defects are believed to originate from the lapping-polishing stages of the substrate preparation.

For the InSb growths, the surface morphology was found to be very sensitive to the V/III ratio and closely reflected the crystallinity of the as-grown films. Based upon the morphology, only a narrow range of V/III ratio around 11 at 465°C was found to be optimum. At a lower V/III ratio around 9, the morphology degraded and the surface was covered with indium droplets; the latter phenomena was confirmed by dissolution of these droplets in hydrochloric acid, which preferentially etches indium. With an increase in V/III ratio the droplets were replaced by hillocks whose density decreased as the ratio reached its optimum value.

Similar studies of the V/III ratio dependence on surface morphology have also been carried out at other temperatures. The optimum condition varied with temperature but similar morphology changes were noticed relative to the optimum point. Optimum V/III ratio increases with decreasing growth temperature. This is due to incomplete decomposition of TMSb at the investigated temperatures. While TMIn completely decomposes around 425°C, TMSb only starts decomposing at 400°C with increasing decomposition efficiency as the temperature increases. hence, higher TMSb flow is required (higher V/III ratio) to compensate for the inefficient decomposition at lower temperatures and as a result, expensive source material is wasted. This might suggest for an increase in the growth temperature but a significant increase is not possible because of the low melting point of InSb (525°C). Growth carried out at temperatures close to the melting point should be avoided since poor quality films are obtained from thermal degradation. Based on these facts and results, the optimum growth temperature and parameters have been determined and they are summarized in Table 1.

Table I: Optimum growth conditions for InSb

Growth temperature	465°C
Growth pressure	76 Torr
TMIn flow rate	50cc/min
TMSb flow rate	20cc/min
Total H_2 flow rate	1.5 ℓ/min

Characterization

Under the optimum conditions, mirror-like InSb epilayers were grown on InSb, GaAs and GaAs-coated Si substrates. Because these films on InSb are lattice matched, they are expected to yield better overall film quality than the ones grown on GaAs and Si. This was confirmed from the comparison of X-ray FWHM of 3 μm-thick InSb films, given in Figure 1. The film grown on InSb had X-ray FWHM of 14 arsec while those grown on GaAs and GaAs/Si exhibited FWHM of 171 and 361 arsec, respectively. The broader peaks on GaAs and Si substrates are due to higher dislocation density. Nevertheless, these FWHM values are one of the best reported for InSb films of comparable thickness on the respective substrates, independent of the growth technology.

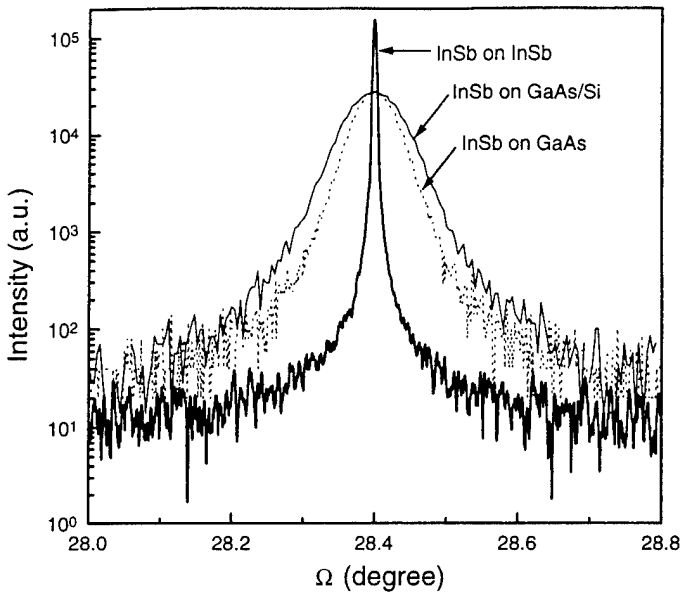

Figure 1: X-ray diffraction spectra of 3.0 μm-thick InSb films grown on InSb, GaAs, and GaAs-coated Si substrates.

For films grown on lattice mismatched substrates, the overall crystalline quality of the film is expected to depend on its thickness. Therefore, X-ray diffraction measurements were performed on InSb films of varying thickness on GaAs and Si substrates and the results are presented in Figure 2. The FWHM of InSb grown on both substrates decreases with increasing film thickness, indicating improved crystalline quality away from the highly mismatched epilayer-substrate interface.

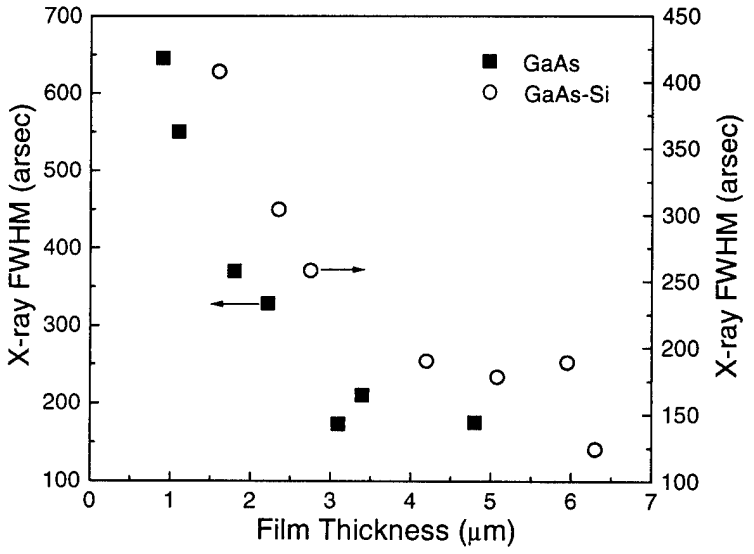

Figure 2: Dependence of the X-ray FWHM of heteroepitaxial InSb layers on film thickness.

The electrical properties of the epilayers were investigated through Hall measurements using Van der Pauw method on clover-shaped samples. The ohmic contacts are made on the samples by alloying with In-Sn at 350 °C under 10% H_2 : 90% N_2 ambient. The current and magnetic field directions are separately reversed to eliminate any Hall-probe misalignment.

Figure 3 shows the room temperature Hall mobility for InSb films grown on GaAs substrates. The Hall mobility is found to improve with increasing thickness. Similar to the X-ray results, this trend reflects the decrease of dislocation density away from the interface. The Hall coefficient R_H was negative and the carrier concentration of the InSb films was generally in the range of $1\times10^{16}cm^{-3}$ to $3\times10^{16}cm^{-3}$ at 300 K. The Hall coefficient remained negative at 77 K but the Hall mobility decreased dramatically far below expected values for n-type InSb. This might indicate that the as-grown layer is p-type. To identify this, more detailed analysis on this behavior has been done using the three-layer model consisting of a surface electron accumulation layer as postulated by Soderstrom et al., an interface layer with high density of dislocations , and a bulk like layer with a highly reduced defect density. The theoretical results with the assumption of p-type InSb layer showed good agreement with the experimental observations verifying the growth of p-type InSb on GaAs substrates.

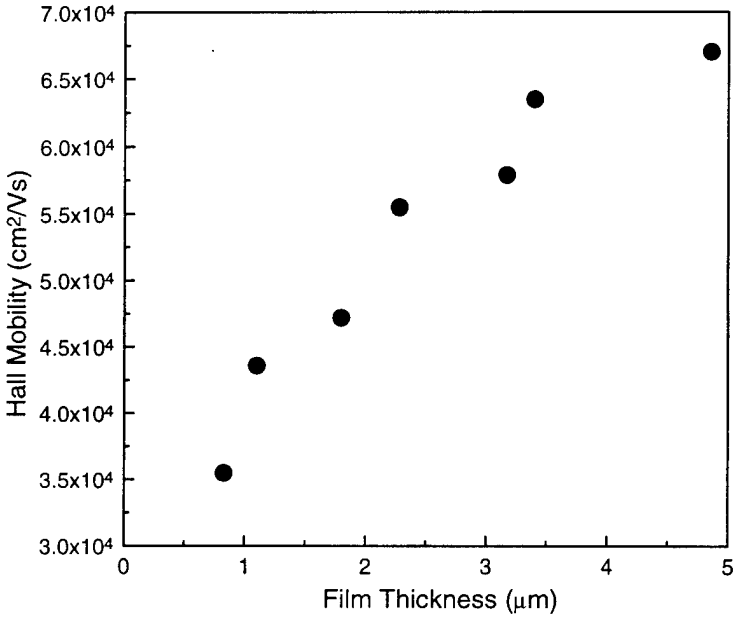

Figure 3: Variation of room temperature Hall mobility of heteroepitaxial InSb layers as a function of film thickness.

In an attempt to improve the electrical properties, a special-grade TMSb was used instead of the electronic-grade TMSb. Using the new source, InSb films with thickness ranging from 1.2 μm to 3.6 μm were grown under the identical conditions of previous growths. The structural quality determined from X-ray rocking curve was comparable and no noticeable change in the room temperature Hall mobilities were observed compared to previous samples grown with electronic-grade TMSb. The most striking differences were the low temperature electrical

characteristics, as shown in Figure 4. The Hall mobility of the new InSb films remained relatively low for film thicknesses below 2 μm but it drastically improved beyond this thickness. A 3.6 μm-thick InSb films exhibited mobility of 56,000 cm^2/Vs at 300 K which increased to about 80,000 cm^2/Vs at 77 K. This temperature dependence of the Hall data differs considerably from our previous results and in fact resembles that of a n-type bulk material. The background carrier concentration at 77 K was comparable to the previous InSb samples up to 2 μm in film thickness but decreased by nearly an order of magnitude to $10^{15}cm^{-3}$ for thicker samples. These Hall data are comparable to the best epitaxially grown InSb results, irrespective of the growth technique.

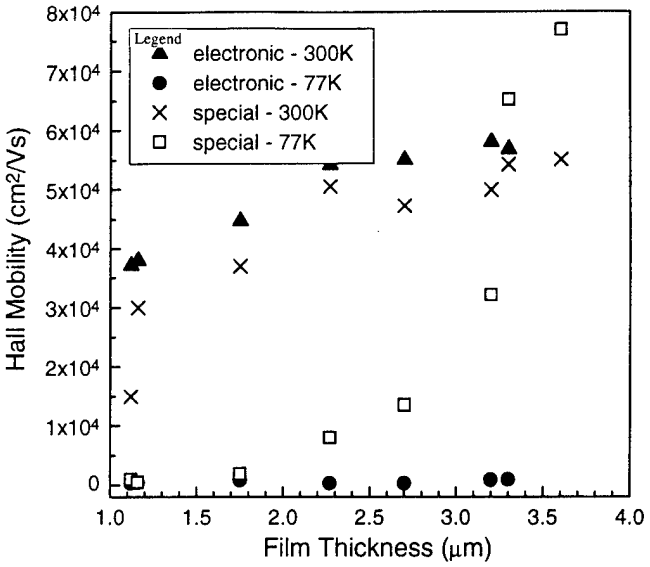

Figure 4(a): Comparison of 300K and 77K Hall mobility of undoped InSb grown using electronic- and special-grade TMSb

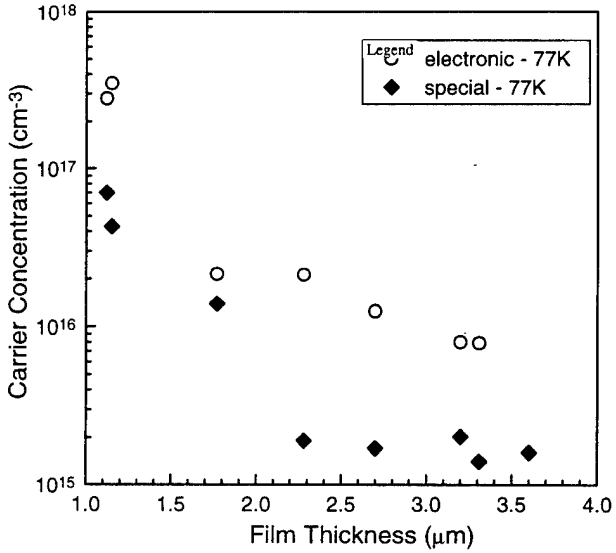

Figure 4(b): Comparison of the 77K carrier concentration of nominally undoped InSb grown using electronic- and special-grade TMSb.

Since the growth conditions and environment are identical between the previous growth with electronic-grade TMSb and the new series of growth with special-grade TMSb, the changes in electrical properties are attributed to an absence of some impurities in the special-grade TMSb that were otherwise present in the electronic-grade TMSb. The impurities, which have not yet been identified, most likely provided a strong p-type background in the old samples. In the new samples, the background is predicted to be n-type since the Hall measurements reflected the high-mobility electron characteristics.

2. Demonstration of the first growth of InTlSb

Cyclopentadienylthallium (CPTl) was used as the source of thallium. CPTl is a solid with low vapor pressure at room temperature and sublimes at 120 °C in vacuum (~0.1 torr). It has been previously used for growing thallium(III) oxide, a compound that has drawn interest with the discovery of high-temperature superconducting Tl-Ba-Ca-Cu oxide. Thallium flow was introduced into the growth chamber without perturbing other growth parameter settings.

This has led to the first successful growth of InTlSb. The InTlSb layer was grown on top of an InSb buffer layer. The thallium incorporation was confirmed through several independent measurements: x-ray diffraction, Auger electron spectroscopy, and optical measurements. The x-ray profile taken at (800) diffraction orientation showed resolved peaks corresponding to InSb and InTlSb (Figure 5). As compared to an InSb reference Auger spectrum, the spectrum of InTlSb exhibited an additional peak associated to thallium[9]. However, the absolute composition of the alloy could not be determined since a InTlSb with known Tl concentration is not available for calibration purpose.

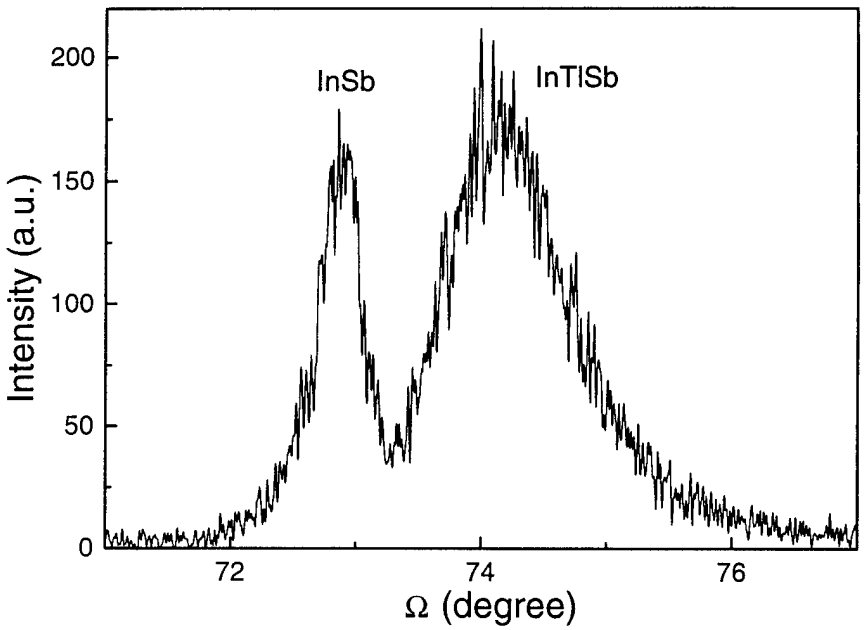

Figure 5: X-ray diffraction profile of InTlSb/InSb samples at (800) orientation.

Once the successful growth of InTlSb has been proven, Tl flow was varied to grow InTlSb alloys of different Tl composition. From the X-ray measurements, the peak corresponding to InTlSb was observed to broaden and shift away from the InSb peak as the thallium content was increased. The InSb peak remained at the same angular position. The broadening trend is clearly reflected in Figure 6 which plots the FWHM of InTlSb peak as a function of the lattice mismatch $\Delta a/a$ between InSb and InTlSb. Both the FWHM and the mismatch were obtained directly from the X-ray profile. The broadening of the InTlSb peak has been attributed to an increase in the dislocation density arising from the increased mismatch with InSb as the thallium concentration increases.

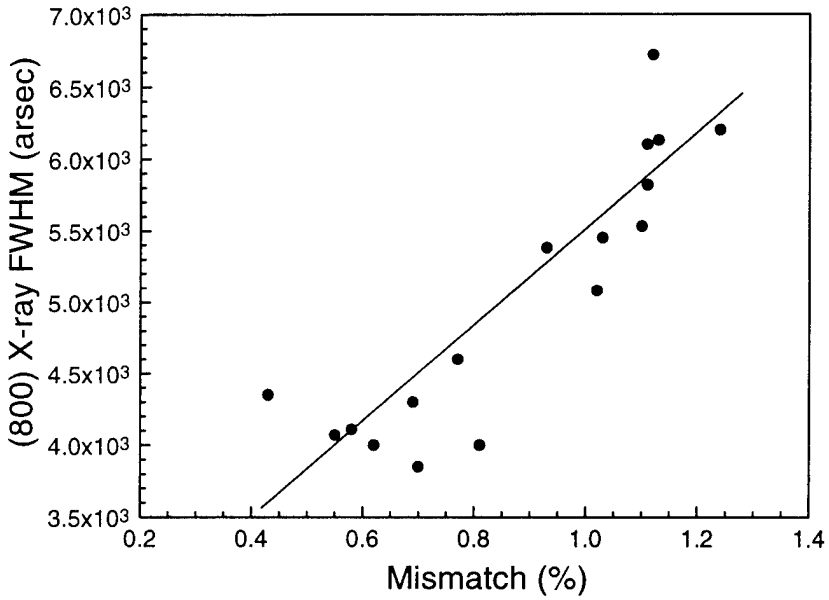

Figure 6: (800) X-ray FWHM of InTlSb layer as a function of its lattice mismatch with InSb.

Electrical characterization of InTlSb samples have shown the Hall data to be sensitive to the growth condition, in particular the thaillium flow. As shown in Figure 7, for the range of InTlSb samples we have investigated, room temperature Hall mobility ranged from $2x10^4 cm^2/Vs$ to $5x10^4 cm^2/Vs$, and an electron concentration ranging from $1x10^{16} cm^{-3}$ to $5x10^{16} cm^{-3}$. Since a direct assessment of thallium is not possible at this time, the lattice mismatch between InTlSb and InSb has been used as an indirect indicator of thallium content in the material. The Hall mobility decreased monotonically with increasing thallium flow, while the electron concentration simultaneously increased. The increase in electron concentration is typical of an intrinsic semiconductor with decreasing bandgap. The decrease in mobility is attributed to an increase in alloy scattering with increasing Tl content.

Measurements at 77 K indicate an opposite trend for the mobility and scattered data for the electron concentration. This behavior is likely to occur because of the multiple contribution of parallel conduction channels which can provide misleading conclusion to the mobility, and carrier type and concentration measured using Hall system. This can be especially true in our InTlSb samples whose non-specular surface can increase surface states and conduction. In

addition, the presence of InSb buffer layer introduce an additional complexity to the analysis of the electrical data.

In order to confirm the bandgap shift, photoconductivity measurements have been performed on the InTlSb/InSb samples. The shape of the spectral response was independent of the bias applied to the photoconductor. Figure 7 shows the normalized spectral response of the InTlSb samples at 77 K. Photoresponse with an onset wavelength up to 9.5μm has been obtained. In general agreement with the theoretical prediction, the samples grown at higher Tl flows exhibited longer response wavelengths.

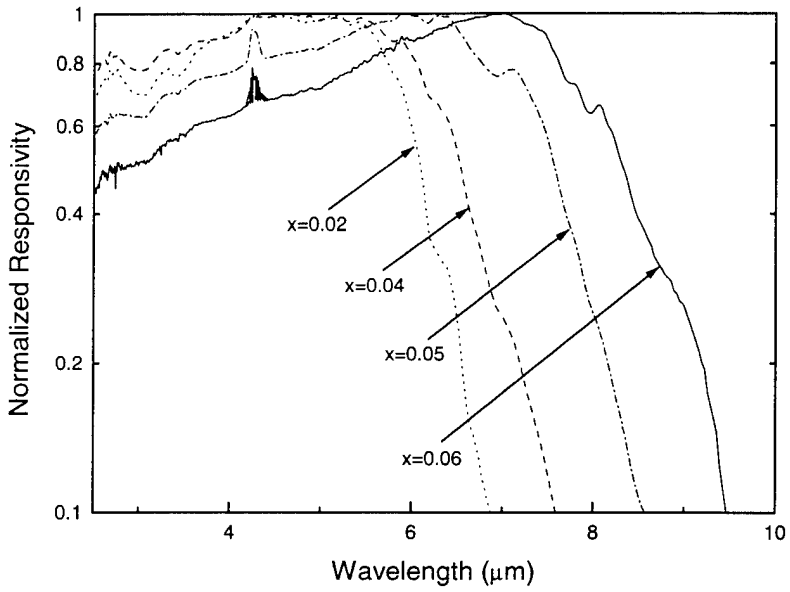

Figure 7: The normalized spectral response of the $In_{1-x}Tl_xSb$ photoconductors at 77 K.

The relationship of increasing photoresponse onset wavelength, and thus increasing thallium composition, to the lattice mismatch (Δa/a) was evidenced in Figure 8. The cut-off wavelength has been determined as the wavelength for which the photoresponse falls at 10 % of its maximum value. A quasi-linear dependence is observed between the photoresponse cut-off wavelength and lattice mismatch, suggesting that the cut-off wavelength can be further extended with increasing thallium content. Furthermore, a 9.5 μm cut-off wavelength corresponds to a lattice mismatch of approximately -1.3 % which is smaller than for an InAsSb alloy having a similar cut-off wavelength. This is important for the development of device-quality material with reduced dislocation density.

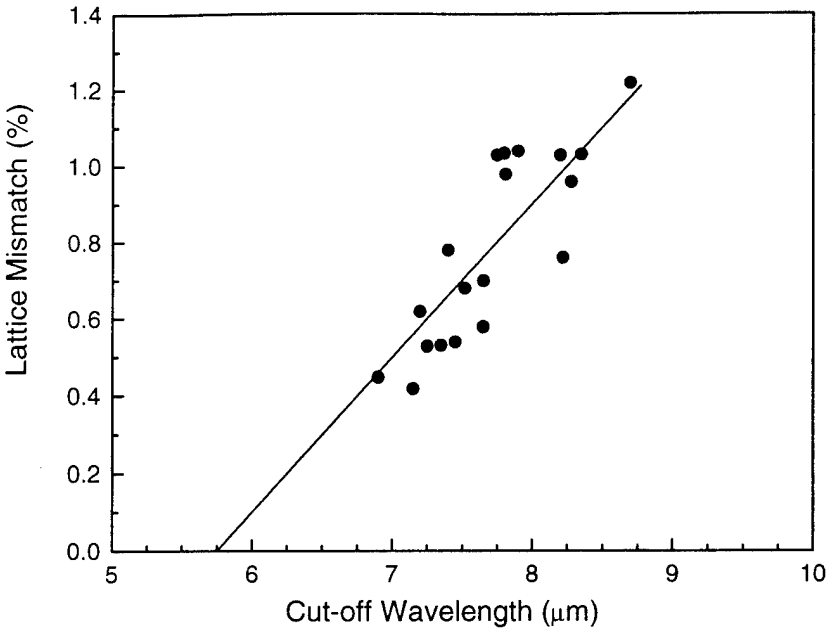

Figure 8: Dependence of the lattice mismatch between InTlSb and InSb on the 77K cut-off wavelength of InTlSb. The cut-off has been determined as the wavelength for which the photoresponse falls at 10 % of its maximum value.

Task 2 InTlSb Doping and Contact

3. Doping of InSb, InAsSb and InTlSb

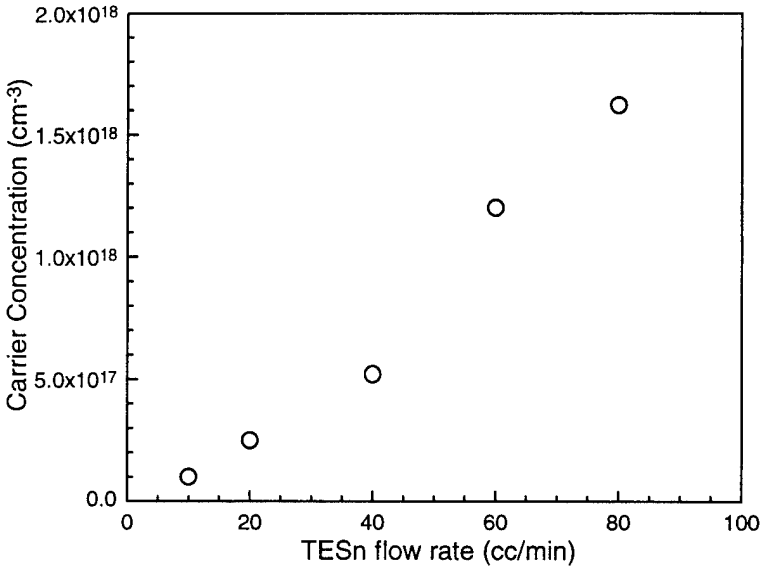

Figure 9: N-type doping concentration dependence on TESn flow rate.

Following the work of Biefeld et al.[15], tetraethyltin (TESn) was used as an n-type dopant source. The TESn was kept at a temperature of -25 °C and the flow rate was varied from 7 cc/min to

80 cc/min, resulting in doping levels ranging from $5 \times 10^{16}cm^{-3}$ to $1.2 \times 10^{18}cm^{-3}$ (Fig. 9). No degradation in surface morphology and x-ray FWHM were observed. Furthermore, we did not notice any memory effect associated with TESn, consistent with the reported work[15]. In order to access the activation energy of Sn dopant in InSb, the carrier concentration (log scale) as a function of temperature has been plotted. Using the relation that the ionized carrier concentration is proportional to exp(-Ei/kT), where Ei is the activation energy, k is the Boltzmann's constant and T is the temperature, Ei has roughly been estimated to be a few tenth of meV.

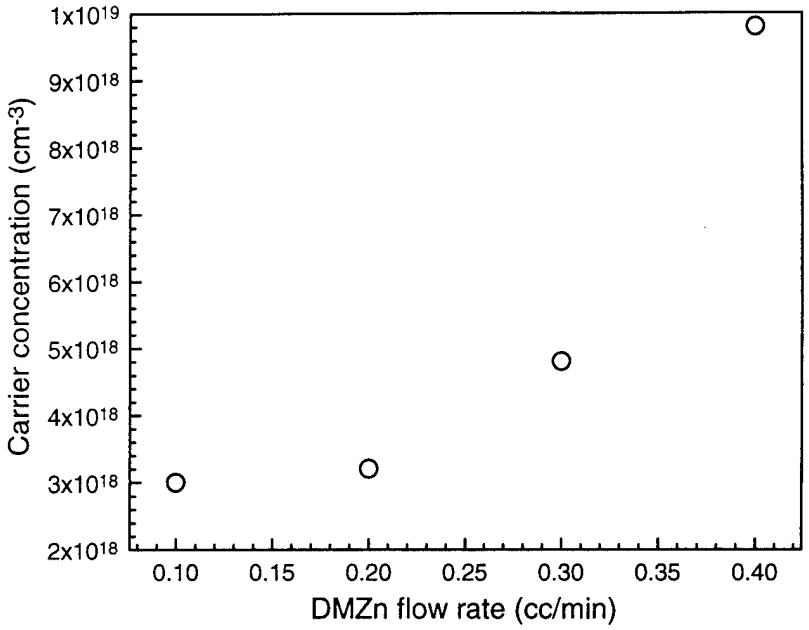

Figure 10: P-type doping concentration as a function of DMZn flow rate.

P-type doping of InSb was first carried out using dimethylzinc (DMZn). Its bubbler was maintained at a constant temperature at -25 °C. The zinc flow was diluted after passing through the bubbler. The dilution flow was kept at 1200 cc/min. Using a 100 cc/min capacity mass flow controller, only concentrations greater than $8 \times 10^{18}cm^{-3}$ were obtained. In order to have a better flow rate control, a smaller capacity mass flow controller (10cc/min) was installed. This enabled us to lower the doping concentration to approximately $3 \times 10^{18}cm^{-3}$ (Fig. 10).

To further extend our doping ranges to lower levels, diethylzinc (DEZn) has been purchased to replace DMZn. DEZn has a much lower vapor pressure than DMZn and is the preferred zinc source for p-type doping of III-V epitaxial alloys. The DEZn bubbler has been kept at 10 °C and the flow was varied from 0.1 cc/min to 0.45 cc/min. The corresponding doping level from $8.26 \times 10^{16}cm^{-3}$ to $1.31 \times 10^{18}cm^{-3}$ has been achieved (Fig. 11). Even lower doping level of $3.06 \times 10^{16}cm^{-3}$ has been achieved by lowering the DEZn bubbler temperature down to -15°C and flowing 0.20 cc/min hydrogen. From the log plot of carrier concentration as a function of temperature, the activation energy of Zn in InSb has been estimated to be a few meV.

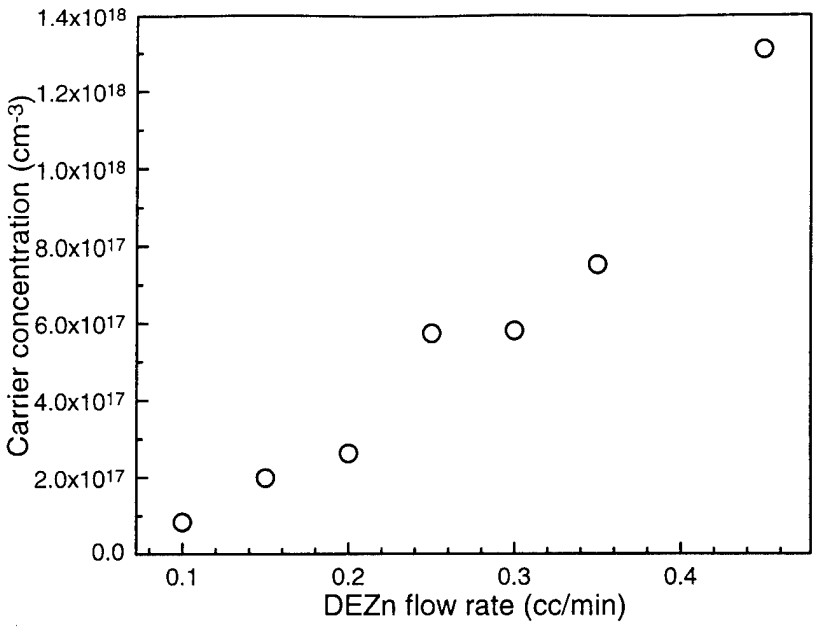

Figure 11: P-type doping concentration as a function of DEZn flow rate.

Once the doping of InSb has been realized, doping of InAsSb and InTlSb epitaxial films has been attempted using the same dopant sources. Even though no systematic studies on the doping of these alloys have been performed, several experimental results showed the similar doping characteristics for InSb, InAsSb and InTlSb using Sn and Zn.

4. Development of Device Processing Technology

4.1 Etching

The first step in fabrication of photodetector is to etch the mesa structure. It was performed using photolithography and wet chemical etching techniques. The mesa size has been determined to be $400\ \mu m \times 400\ \mu m$ including the $100\ \mu m \times 100\ \mu m$ contact area. The Shipley 1813 photoresistance has been used for the photolithography process. The etching rate and mesa height has been measured by alpha step machine (Tencor). After prebake at 90 °C the wafer has been exposed to UV light (Kark-Suss) for 12 seconds and developed by Shipley Developer 351 for about 1 min. The post-bake was done at 120 °C for 30 min. The etching solutions were lactic:nitric acid and it was etched at room temperature.

4.2 Metallization

Metallization was realized by an e-beam evaporator. After several trial, the metallization step has been determined. Ti/Au contact has been suggested because Ti is strongly adhesive to the semiconductor surfaces and chemically stable. It formed good ohmic contact to both n-and p-type materials. The photolithography technique was employed to get the contact pattern. The etching solutions for Au ($KI:I_2:H_2O$) and Ti (HF) are selective. Furthermore, the etching solutions for Ti (HF) and InSb (lactic:nitric) are also selective. Thus, it provides us a good way to protect the surface of InSb when the contact pattern is made by chemical etching.

4.3 Wire bonding and mounting

The fabricated chips are mounted on the copper heat sink coated with In at a temperature of 160 °C in an ambient gas of 90 % N_2 and 10 % H_2 for 2 min. Au ball bonding has been done by Au ball bonding machine. Since InSb is mechanically soft, special care had to be taken by adjusting the force, power, time temperature during the bonding. More effort will be given to the improvement of bonding technology because the InTlSb is softer and Ti is less adhesive to this material than InSb.

Task 3 Fabrication of Detectors

5. InTlSb photoconductors on GaAs

The photoconductors were rectangular shaped with dimension of 3×3 mm^2. Ti/Au were evaporated by an electron-beam evaporator to make ohmic contacts. Ti exhibits strong mechanical adhesion with semiconductor materials. The resistance was about 50 ohms at room temperature and increased up to several thousand ohms at 77 K. The spectral photoresponse was measured by a FTIR spectrometer with a low-noise preamplifier (Ithaco 120). The responsivity was calibrated by a blackbody test set-up, including a blackbody source, preamplifier, and chopper system. The blackbody temperature was set at 800 K. The modulating frequency was set at 400 Hz since response measurements as a function of chopper frequency showed that the thermal effect could be neglected at frequencies higher than 200 Hz.

Figure 7 in the previous section shows the spectral response of $In_{1-x}Tl_xSb$ (with estimated $0.02 \le x \le 0.06$) photodetectors at 77 K, which is normalized to the peak responsivity. The cut-off wavelengths are clearly seen in the $In_{1-x}Tl_xSb$ photodetectors, which extend to long wavelengths with increasing Tl content. The absolute responsivity for an $In_{0.04}Tl_{0.06}Sb$ photodetector is displayed in Figure 12. The cut-off wavelength extends up to 11 μm at 300 K. The maximum responsivity in an $In_{0.065}Tl_{0.035}Sb$ photodetector is about 6.64 V/W at 77 K. The corresponding Johnson-noise limited detectivity is 7.64×10^8 cm·$Hz^{1/2}$/W. The voltage responsivity and detectivity of $In_{1-x}Tl_xSb$ photodetectors are listed in Table II.

Table II: The performance of the $In_{1-x}Tl_xSb$ photoconductors at 77 K.

$In_{1-x}Tl_xSb$ detectors	$\lambda_{cut\text{-}off}$ (μm)	R_v^{max} (V/W)	D^*_{max} (cm·$Hz^{1/2}$/W)	μ (cm^2/V·s)	τ (ns)
x=0.02	6.5	2.73	2.47×10^8	1.29×10^3	19.2
x=0.04	7.3	6.64	7.64×10^8	2.00×10^3	50.1
x=0.05	8.4	3.56	8.54×10^8	2.75×10^3	40.4
x=0.06	9.4	0.79	2.63×10^8	4.13×10^3	10.3

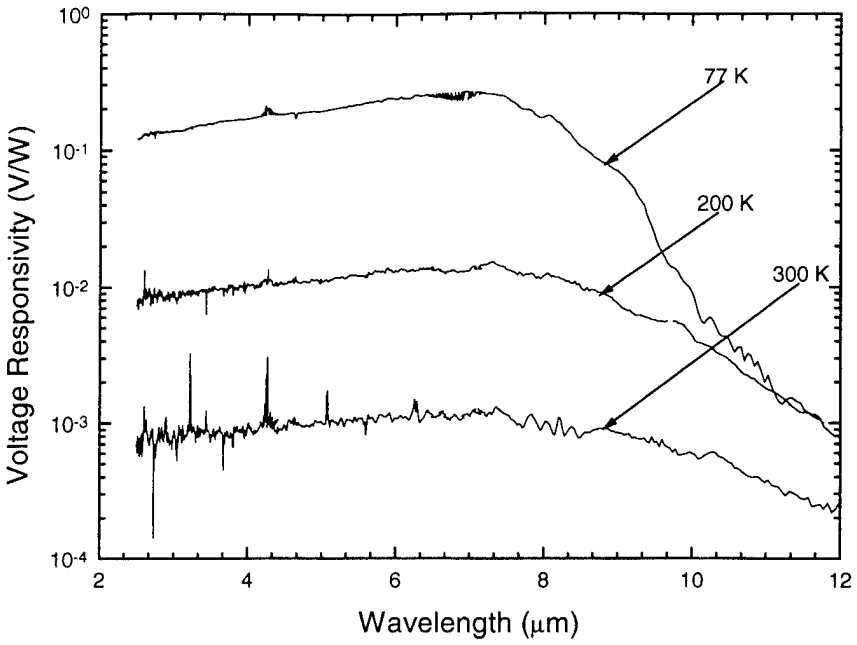

Figure 12: The spectral responsivity of $In_{0.04}Tl_{0.06}Sb$ photoconductor at 77 K, 200 K, and 300 K.

In order to get the carrier lifetime τ, the voltage-dependent responsivity was measured. Figure 13 shows the voltage-dependent responsivity of InTlSb photodetectors. It increases with voltage, saturates at a given voltage, and finally decreases. The saturation responsivity at large voltage can be explained by the sweep-out effect[13]. Based on the voltage-dependent responsivity, τ can be derived according to the simple theory of photoconductivity[14]. The voltage responsivity can be expressed as

$$R_v = \frac{q\lambda}{hc}\frac{\eta\mu_e\tau V_b R_D}{L^2}\left(1+\frac{1}{b}\right) \qquad (1)$$

where q is the electron charge, λ is the incident wavelength, μ_e is electron mobility, η is the quantum efficiency, b is the ratio of the electron-to-hole mobility, L is the detector length, V_b is the bias voltage, and R_D is the detector resistance. The quantum efficiency η can be obtained by

$$\eta = (1-r)\frac{\left(1-e^{-\alpha t}\right)}{\left(1-re^{-\alpha t}\right)} \qquad (2)$$

where r is the reflectivity, α is the absorption coefficient, and t is the detector thickness. The quantum efficiency is estimated to be 64 %.

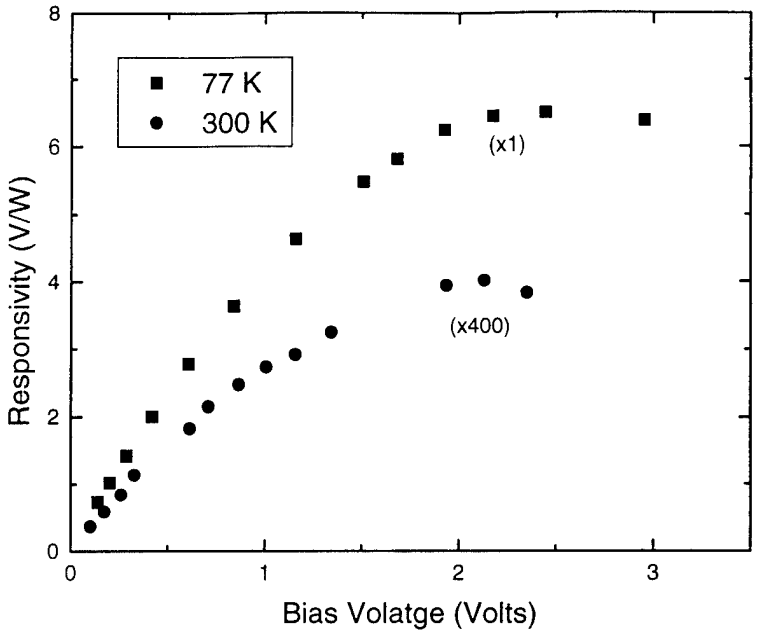

Figure 13: The voltage-dependent responsivity of an $In_{0.06}Tl_{0.04}Sb$ photoconductor.

The effective lifetime τ in InTlSb epitaxial layers is listed in Table II, which is 10-50 ns at 77 K. At 300 K, D^* is 10^6-10^7 cm·$Hz^{1/2}$/W and τ is 0.1-0.6 ns.

6. Photovoltaic detector Performance Measurement

For the focal plane array applications, photovoltaic devices are necessary because it requires no bias which results in the reduced thermal heating. To develop the technical line for the future InTlSb photodiode applications, well established materials such as InSb and InAsSb photodiode have been fabricated using device processing step described above. The performance of the photodiode has also been measured.

6.1 Photodiode measurement set up

The current voltage characteristics has been measured by Hewlett Packard I-V tracer. In order to analyze the dark current mechanisms in the devices, temperature dependent R_0A product has also been measured within a small current of μA order between 77 K and 300 K. The spectral response measurement were carried out by a Mattson FTIR spectrometer. Absolute responsivity has been obtained using the blackbody test set up described in the section 1 of this report.

6.2 InSb photovoltaic detector

Both n-i-p and p-i-n structures have been examined for the InSb photovoltaic detector. Absolute spectral responsivities of these detectors are given in the following. Both detector showed the photoresponse up to 5.5 μm at 77 K and 7.5 μm at 300 K. As is clearly seen from the graph, p-i-n structure gave responsivities almost two orders of magnitude higher than n-i-p structure. We think that in the n-i-p structure the p-n junction is closer to the substrate and this might result in the lower performance. When p-n junction is closer to the substrate side, the junction can have

more defect density and at the same time the incident photon flux can be reduced by the absorption from the top n-type and intrinsic layer. Further study should be done to understand this results because it is important for the detector structure determination of the InTlSb photovoltaic detectors.

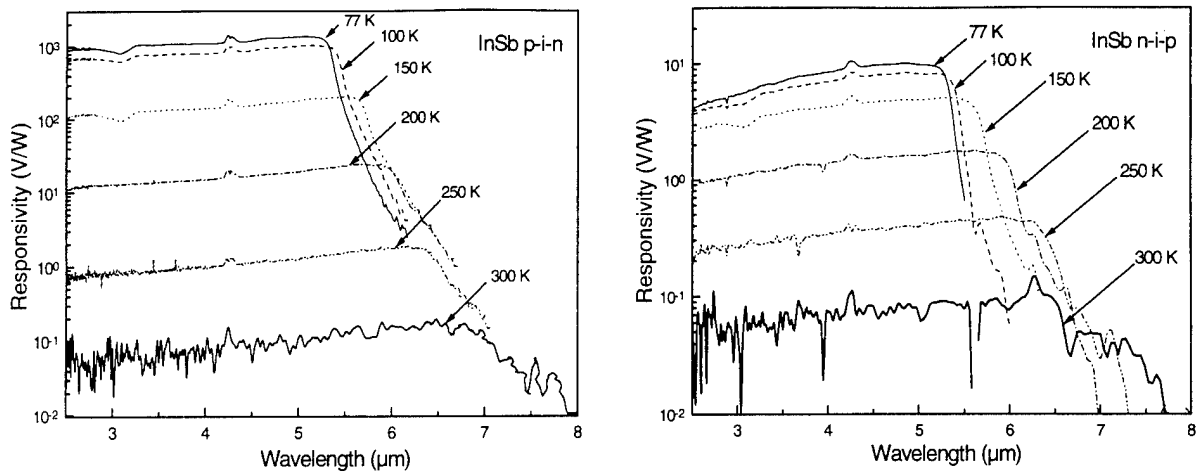

Figure 14: Photoresponse of InSb photodiodes with different structures (p-i-n and n-i-p).

4.3 InAsSb photovoltaic detector

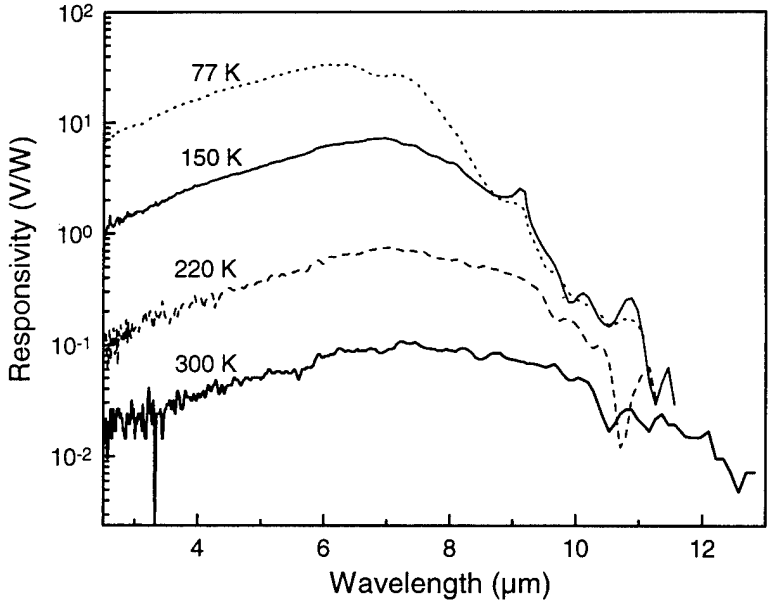

Figure 15: Photoresponse of p-π-n InSb/$InAs_{0.15}Sb_{0.85}$/InSb double heterojunction photodiode.

As a first step for the longer wavelength photovoltaic detector applications, InAsSb was investigated first because it is well developed system. As InTlSb material system and the detector from it are expected to be similar to those from InAsSb, the investigation of InAsSb system is

worth doing. At the same time InAsSb can make competition with HgCdTe for near room temperature operation at 8-12 μm spectral range. Work performed at CQD showed well behaved InAsSb photodiode. p^+-InSb/p^--$InAs_{1-x}Sb_x$/n^+-InSb double heterojunction photodiodes operated at near room temperature in the 8-13 μm region of infrared spectrum[4]. A room temperature photovoltaic response of up to 13 μm has been observed at 300 K with an $x \approx 0.85$ sample as shown in Figure 15. The voltage responsivity-area product of $3 \times 10^{-5} Vcm^2/W$ has been obtained at 300 K for the 10.6 μm optimized device.

4.4 InTlSb photovoltaic detector

In order to approach the InTlSb photovoltaic detectors, InSb/InTlSb/InSb p-i-n double heterostructures were suggested. The doping level for the p-type contact layer was $5 \times 10^{18} cm^{-3}$ and n-type layer was $5 \times 10^{16} cm^{-3}$. Almost same processing step as that for InSb detector has been used. Even though the surface of the layer was rough, Ti/Au metals made good contact with the surface. Wire bonding was achieved with Au-ball bonding machine but with more care than InSb case. The spectral response was obtained only up to 5.5 μm indicating no response from the InTlSb layer.

CONCLUSION

In this work, growth and material properties of InSb and InTlSb epitaxial films have been investigated and their potentials for infrared detection have been explored. High quality InSb films were grown on lattice mismatched GaAs and GaAs-coated Si substrates using TMI and TMSb as indium and antimony sources.

Reproducible growth of InTlSb has been achieved. Variation of Tl composition by changing the Tl flow or Sb flow has been obtained and InTlSb layers with different Tl compositions have been directly grown on semi-insulating GaAs substrate. Photoconductors have been fabricated by depositing Au/Ti on the edges of the rectangular shaped InTlSb samples. The detector performance has been measured. Corresponding calculation for the effective carrier lifetime (τ) and estimated detectivity(D^*) resulted in the τ of 10-50 ns and D^* of $2\text{-}9 \times 10^8 cm \cdot Hz^{1/2}/W$ at 77K. At 300 K, D^* was $10^6\text{-}10^7$ $cm \cdot Hz^{1/2}/W$ and τ was 0.1-0.6 ns.

Systematic doping studies have been don for InSb. Using DEZn lower p-type doping level of $3 \times 10^{16} cm^{-3}$ has been achieved. Similarity of doping characteristics for InAsSb and InTlSb have also been verified. Using the established growth techniques and doping level control, InSb and InAsSb photovoltaic detectors have been demonstrated. During the fabrication of those detectors, processing technology for the InSb based materials has also been developed. Preliminary InTlSb photovoltaic detector has also been fabricated.

Throughout this study we discovered the feasibility of various III-V semiconductors for the LWIR applications. They include InTlSb, InAsSb, and InSbBi compounds. Because of their possibility to replace the current leading HgCdTe material system, the subject is very exciting and needs to be continued. The continuing work will be performed at the Center for Quantum Devices.

REFERENCES

1. Y. H. Choi, R. Sudharsanan, C. Besicki, E. Bigan, and M. Razeghi, Mat. Res. Soc. Symp. Proc. 281, 375,1993.
2. C. Besicki, Y. H. Choi, R. Sudharsanan, and M. Razeghi, J. Appl. Phys. 73, 5009, 1993.
3. S. N. Song, J. B. Ketterson, Y. H. Choi, R. Sudharsanan, and M. Razeghi, Appl. Phys. Lett. 63, 964, 1993.
4. J. D. Kim, S. Kim, D. Wu, J. Wojkowski, J. Xu, J. Piotrowski, E. Bigan, and M. Razeghi, Appl. Phys. Lett. 67, 2645, 1995
5. J. D. Kim, D. Wu, J. Wojkowski, S. J. Park, Y. H. Choi, J. Xu, J. Piotrowski, and M. Razeghi, 188th Electrochemical Society Meeting, Chicago, Illinois, October, (1995).
6. J. D. Kim, D. Wu, J. Wojkowski, J. Piotrowski, J. Xu, and M. Razeghi, Appl. Phys. Lett. 68, 99, 1996.
7. Y. H. Choi, C. Besicki, R. Sudharsanan, and M. Razeghi, Appl. Phys. Lett. 63, 361, 1993
8. M. Razeghi, Y. H. Choi, P. T. Staveteig, and E. Bigan, Proceedings of the 184th meeting of the Electrochemical Society, New Orleans, Lousiana, October, 1993.
9. Y. H. Choi, P. T. Staveteig, E. Bigan, and M. Razeghi, J. Appl. Phys. 75, 3196, 1994.
10. P. T. Staveteig, Y. H. Choi, G. Labeyrie, E. Bigan, and M. Razeghi, Appl. Phys. Lett. 64, 460, 1994.
11. E. Bigan, Y. H. Choi, G. Labeyrie, and M. Razeghi, Proceedings of SPIE, Los Angeles, California, January 1994.
12. J. D. Kim, E. Michel, S. Park, J. Xu, S. Javadpour, and M. Razeghi, submitted to Appl. Phys. Lett. for publication
13. A. Rogalski, "Infrared Photon Detectors", SPIE, Bellingham, Washington, 1995.
14. S. M. Sze, "Physics of Semiconductor Devices (2nd edition)", Wiley, New York, 1981.
15. R. M. Biefeld, J. R. Wendt, and S. R. Kurtz, J. of Crystal Growth 107, 836, 1991.

LIST OF PUBLICATIONS

- Y. H. Choi, R. Sudharsanan, C. Besicki, E. Bigan, and M. Razeghi, Mat. Res Soc. Symp. Proc. 281, 375, (1993).
- C. Besicki, Y. H. Choi, R. Sudharsanan, and M. Razeghi, J. Appl. Phys. **73**, 5009, (1993).
- S. N. Song, J. B. Ketterson, Y. H. Choi, R. Sudharsanan, and M. Razeghi, Appl. Phys. Lett. **63**, 964, (1993).
- Y. H. Choi, C. Besicki, R. Sudharsanan, and M. Razeghi, Appl. Phys. Lett. **63**, 361, (1993).
- M. Razeghi, Y. H. Choi, P. T. Staveteig, and E. Bigan, Proceedings of the 184th Meeting of the Electrochemical Society, New Orleans, Lousiana, October, (1993).
- Y. H. Choi, G. Labeyrie, P. T. Staveteig, E. Bigan, and M. Razeghi, Proceedings of the 184th Meeting of the Electrochemical Society, New Orleans, Lousiana, October, (1993).
- Y. H. Choi, "InTlSb for 8-12μm range detector," PhD qualifying exam, Northwestern university, Department of electrical engineering and computer science, (1993).
- Y. H. Choi, P. T. Staveteig, E. Bigan, and M. Razeghi, J. Appl. Phys. **75**, (1994).
- E. Bigan, Y. H. Choi, G. Labeyrie, and M. Razeghi, Proceedings of SPIE, LosAngeles, California, (1994).
- P. T. Staveteig, Y. H. Choi, G. Labeyrie, E. Bigan, and M. Razeghi, Appl. Phys. Lett. **64**, 460, (1994).
- M. Razeghi, Y. H. Choi, J. D. Kim, and E. Bigan, Electrochamical Society, Miami, Florida, October, (1994).
- M. Razeghi, "Organo-Metallic Vapor Phase Epitaxy of Semiconductors," chapter in Handbook on Semiconductors, Second Edition, Volume3: Materials, Properties and Preparations.
- E. Michel, G. Singh, S. Slivken, C. Besicki, P. Bove, I Ferguson, and M. Razeghi, Appl. Phys. Lett., **65**, 3338 (1994).
- G. Singh. E. Michel, C. Jelen, S. Slivken, J. Xu, P. Bove, I. Ferguson, and M. Razeghi, J. Vac. Sci. Technol. B, **13**, 783 (1995).
- E. Michel, R. Peters, S. Slivken, C. Jelen, P. Bove, J. Xu, I Fergison, and M. Razeghi, Proceedings of the SPIE, **2397**, 379 (1995)
- J. D. Kim, S. Kim, D. Wu, J. Wojkowski, J. Xu, J. Piotrowski, E. Bigan, and M. Razeghi, Appl. Phys. Lett. **67**, 2645 (1995).
- M. Razeghi, J. D. Kim, S. J. Park, Y. H. Choi, D. Wu, E. Michel, J. Xu, and E. Bigan, Proceedings of the 22nd International Symposium on Compound Semiconductors, Cheju Island, Korea, 1085 (1995).
- J. D. Kim, D. Wu, J. Wojkowski, S. J. Park, Y. H. Choi, J. Xu, J. Piotrowski, and M. Razeghi, Proceedings of the 188th Electrochemical Society Meeting, Chicago, Illinois, October, (1995).
- J. D. Kim, D. Wu, J. Wojkowski, J. Piotrowski, J. Xu, and M. Razeghi, Appl. Phys. Lett. **68**, 99 (1996).
- E. Michel, J. Xu, J. D. Kim, I. Ferguson, and M. Razeghi, IEEE Phot. Tech. Lett., **8**, 673 (1996)
- E. Michel, J. D. Kim, S. Park, J. Xu, I Ferguson, and M. Razeghi, Proceedings of the SPIE, **2685**, 105 (1996).

- E. Mihcel, J. D. Kim, J. Xu, I. Ferguson, and M. Razeghi, Appl. Phys. Lett. 69, 215, 1996.
- J. D. Kim, E. Michel, S. J. Park, J. Xu, S. Javadpour, and M. Razeghi, Appl. Phys. Lett. 69, 343, 1996.
- J. J. Lee, J. D. Kim, and M. Razeghi, Accepted for publication, Appl. Phys. Lett., 1997.